JOURNAL OF SOLID STATE CHEMISTRY 62, 360–370 (1986)

The Electronic Structure of $Bi_{2-x}Gd_xRu_2O_7$ and RuO_2: A Study by Electron Spectroscopy

P. A. COX, J. B. GOODENOUGH, P. J. TAVENER, AND D. TELLES

Inorganic Chemistry Laboratory, South Parks Road, Oxford OX1 3QR, United Kingdom

AND R. G. EGDELL*

Department of Chemistry, Imperial College of Science and Technology, South Kensington, London SW7 2AZ, United Kingdom

Received August 12, 1985

The bismuth gadolinium pyrochlore ruthenates $Bi_{2-x}Gd_xRu_2O_7$ have been studied in relation to RuO_2 by the techniques of X-ray and ultraviolet photoelectron spectroscopy (XPS and UPS) and high-resolution electron-energy-loss spectroscopy (HREELS). The composition-dependent metal-to-semiconductor transition in the pyrochlore system is mirrored by the progressive decrease with composition parameter in (i) the density of electronic states at the Fermi energy in UPS, (ii) the plasmon frequency in HREELS, and (iii) the probability of screening a Ru : 3*d* core hole in XPS. These changes are too gradual in themselves to pinpoint the transition, but are generally consistent with transport and X-ray diffraction data that indicate a metal-to-nonmetal transition at $x = 1.55$ mediated by an interplay between disorder and correlation-induced electron localization. Comparison of the results for the pyrochlores with those from RuO_2 suggest that the fine structure in the Ru : 3*d* spectrum of the latter material, previously believed to arise from differing oxidation states at the surface, should in fact be attributed to final-state screening effects in a stoichiometric material. Our conclusion is confirmed by the signals associated with the Ru : 4*d* electrons in XPS, UPS, and HREELS: each of these three techniques appears to probe a conduction-electron concentration essentially equal to its bulk value. In particular, UPS confirms details of the band structure of RuO_2 not obvious from previous photoemission experiments.

1. Introduction

The electronic properties of ruthenium(IV) oxides are both of intrinsic interest and of significance in the technological application of the materials. Ruthenium dioxide itself adopts the undistorted rutile structure and is a metallic conductor with weak Pauli paramagnetism (*1*), but the Ru : 4*d* electrons in ternary ruthenium(IV) oxides sit on the borderline between localized and itinerant behavior. Thus whereas the pyrochlore oxide $Bi_2Ru_2O_7$ is a metallic conductor, $Gd_2Ru_2O_7$ in common with the other rare earth ruthenates and $Y_2Ru_2O_7$ is a semiconductor with a localized t_{2g}^4 4*d* electron configuration (*2*). In a previous publication we have shown that the tech-

* To whom correspondence should be addressed.

0022-4596/86 $3.00

niques of high-resolution electron spectroscopy provide a powerful probe into the electronic structure of materials of this sort and have traced the evolution of electron localization in going from metallic Pauli paramagnetic $Bi_2Ru_2O_7$ and $Pb_2Ru_2O_{7-y}$ through the highly correlated metals $SrRuO_3$ and $CaRuO_3$ to the antiferromagnetic insulator $Y_2Ru_2O_7$ (*3*).

The spectroscopic work provides in turn a basis for understanding the electrochemical behavior of ruthenium(IV) oxides (*4*). This is of particular concern since RuO_2 finds application as an anode for the evolution of both Cl_2 and O_2 (*5*); and pyrochlore lead and bismuth ruthenates (particularly the ruthenium-deficient materials where the *B* metal occupies some of the ruthenium sites) are more effective than noble metals, including platinum, as electrocatalysts in the evolution of oxygen (*6*).

The scope of our earlier work is extended here by a study of electron spectra of the quaternary pyrochlore ruthenates $Bi_{2-x}Gd_xRu_2O_7$. This system exhibits an almost continuous range of compositions between $x = 0$ and $x = 2$, the end members of which are respectively a metal and an insulator. It thus affords the possibility of studying changes in electronic structure accompanying a metal-to-nonmetal transition. In particular, the well-defined evolution of localized electronic states as the gadolinium content increases allows us to appraise the role of final-state effects associated with screening by itinerant electrons upon X-ray photoelectron spectra. It transpires that the data obtained in the present study lead us to revise the assignment of fine structure previously noted in the Ru : 3*d* core-level spectra of metallic RuO_2 (*7–9*). The instrumental resolution achieved in our UPS and electronic EELS measurements is almost an order of magnitude better than is usual in such studies. Thus we are additionally able to make more detailed comparisons between our experimental data and published band-structure calculations for RuO_2 (*10*) than has hitherto been possible.

2. Experimental

The polycrystalline RuO_2 used in the present work was obtained from Koch-Light Limited; it gave an X-ray powder diffraction pattern consistent with literature data (*11*).

The ternary oxides $M_2Ru_2O_7$ (M = Bi or Gd) were prepared by heating stoichiometric mixtures of the appropriate oxide M_2O_3 and RuO_2 in air at temperatures between 900 and 1400 K with frequent regrindings until sharp X-ray powder patterns characteristic of the cubic pyrochlore structure were obtained. Care was taken in the firing cycle to avoid loss of RuO_2 (which volatilizes as RuO_4) or Bi_2O_3. The quaternary oxides $Bi_{2-x}Gd_xRu_2O_7$ were prepared by heating in air mixtures of $Bi_2Ru_2O_7$ and $Gd_2Ru_2O_7$. The firing temperature required to produce a single-phase material increased with gadolinium content. Samples with nominal composition parameter x = 2.0, 1.6, 1.4, 1.0, 0.4, and 0.0 were studied in the present work. It was established by electron microprobe analysis and atomic absorption spectroscopy that the stoichiometry corresponded closely to its nominal value.

Before introduction into the spectrometer, samples were pressed into 13-mm disks between tungsten carbide dies and fired in air at 1070 K for 24 hr to give mechanically robust ceramic pellets. All spectra were recorded at room temperature in an ESCALAB 5 electron spectrometer with facilities for XPS, UPS, and HREELS. Samples were cleaned in the preparation chamber of the spectrometer (base pressure 5×10^{-10} Torr) by annealing at temperatures up to 1100 K under 100 Torr pure oxygen (BOC zero grade). Following transfer to the main chamber, X-ray photoelectron spectra were

found to be free of signals due to carbon or other contaminants and HREEL spectra were free of losses due to unwanted adsorbate molecules.

Sample stoichiometry was monitored *in situ* by measuring intensities of the dominant core peaks in XPS (Gd : 4*d*, Bi : 4*f*, Ru : 3*d*, O : 1*s*). The Gd : 4*d* peak has a complicated band profile (Fig. 1) owing to coupling of the 4*d* photohole with the open 4*f* configuration (*12*). Nonetheless the peak lies close to the simple Bi : 4*f* spin–orbit doublet; after subtraction of structure due to satellite radiation, one can make reasonable estimates of the Gd : 4*d*/Bi : 4*f* intensity ratios without the need to correct the data for variation of the analyzer transmission function. In Fig. 2 the intensity ratio I(Gd : 4*d*)/I(Bi : 4*f*), corrected for the relevant subshell cross sections, is plotted against the nominal Gd/Bi ratio $x/(2-x)$. It is seen that the gadolinium peak becomes progressively stronger as the composition parameter increases although the ratio is always smaller than expected from the composition. Further analysis of our data suggests that one must also recognize an overall enrichment in the counterion (Bi or Gd) relative to Ru. It is uncertain from our measurements whether the effects observed can be entirely attributed to a preference to terminate the surface with Bi (or Gd) rather than Ru in the topmost cation plain: alternatively there is a change in chemical composition close to the surface with occupation of Ru sites by Bi, as in the bulk ruthenium-deficient pyrochlore phases (*6*), and preferential occupation of sites available to the countercations by Bi rather than Gd. Despite the apparent difference between bulk and surface stoichiometry, the electronic properties (in terms of localized versus itinerant electron behavior) of the end members of the pyrochlore series as inferred from UPS, EELS, and XPS measurements are consistent with bulk transport properties. In particular, there is a well-defined evolution of the spectra as the composition parameter varies.

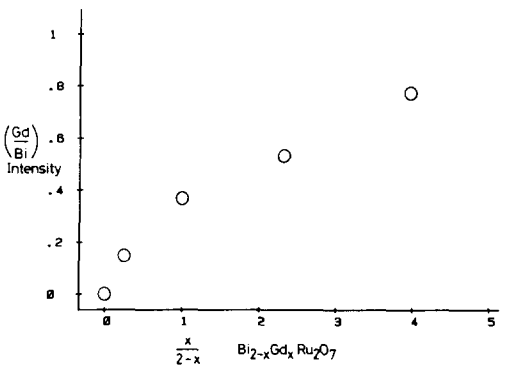

FIG. 2. Intensity ratio of Gd : 4*d* and Bi : 4*f* peaks from Fig. 1 (corrected for subshell ionization cross sections) plotted against the bulk nominal Gd/Bi atomic ratio $x/(2-x)$.

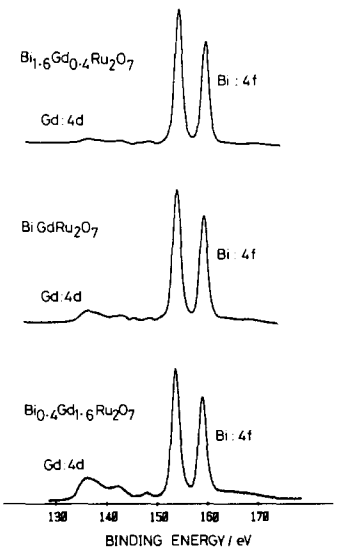

FIG. 1. Mg*Kα* X-ray photoelectron spectra of the pyrochlore ruthenates embracing the Gd : 4*d* and Bi : 4*f* peaks. Structure due to satellite radiation has been subtracted from the spectra.

3. The Band Structure of Pyrochlore Ruthenates

The cubic pyrochlore structure adopted by ternary ruthenates $A_2Ru_2O_6O'$ is based

on a framework of corner-sharing RuO_6 octahedra. In contrast to the simpler perovskite structure, where the Ru–O–Ru angle is 180°, the RuO_6 octahedra in the pyrochlores are linked into zig-zag chains with an Ru–O–Ru angle of around 135°. The A_2O' ions form an interpenetrating anti-SiO_2 array. The octahedral ligand field experienced by the Ru^{4+} ions splits the $4d$ subshell into more stable t_{2g} and less stable e_g components. For many transition metal compounds based on corner-sharing MO_6 octahedra, indirect M–O–M interactions lead to a sufficiently wide t_{2g} band to allow itinerant-electron behavior. However, for both $Y_2Ru_2O_7$ and rare earth ruthenates, including $Gd_2Ru_2O_7$, the relatively unfavorable Ru–O–Ru angle coupled with competition for the O : $2p$ orbitals by the acidic A^{3+} ions yields a t_{2g} band insufficiently wide to sustain itinerant behavior; for these materials one finds a localized t_{2g}^4 configuration at the ruthenium ions, possibly with antiferromagnetic ordering of the localized moments at low temperatures. By contrast, in $Bi_2Ru_2O_7$ where the Bi^{3+} ions have a $6s^2$ valence-electron configuration Bi–O–Ru interactions appear to enhance the width of the Ru : $4d(t_{2g})$ band sufficiently to allow for metallic behavior and Pauli paramagnetism (*13*). The direct involvement of the Bi : $6s$ orbitals in the conduction band of $Bi_2Ru_2O_7$ has been demonstrated in our recent electron spectroscopic measurements on this material (*3, 4*).

Any description of the transition from nonmetallic to metallic behavior as Gd is replaced by Bi must introduce the idea of upper and lower Hubbard bands separated by a well-defined energy gap in the nonmetallic regime. As the transfer integral that characterizes the width of the one-electron t_{2g} band increases with Bi content, the Hubbard bands broaden and eventually coalesce with a sudden jump from zero in the density of electronic states at the Fermi energy (at 0 K). However, one must envisage the possibility of a limited composition regime in which the Hubbard bands overlap, but metallic behavior is suppressed by disorder-induced (Anderson) localization of electronic states in the pseudogap region of band overlap.

In previous work it has been shown that a transition to the metallic state close to $x = 1.55$ may be inferred from conductivity data (*13, 14*). A narrow two-phase region separates metallic materials with $x < 1.4$ from nonmetallic materials with $x > 1.6$. Well-defined Vegard relationships are observed within each regime although there is a change in slope between metallic and nonmetallic phases; the lattice parameter always increases with increasing Bi content but it appears that Bi^{3+} has a bigger effective radius in the nonmetallic state than in the metallic state. This is attributed to transfer of Bi : $6s$ electron density into Ru : $4d$ states in the metallic regime as a result of involvement of the Bi orbitals in the conduction band.

4. He(I) and HREEL Spectra of the Pyrochlore Ruthenates

Wide-scan He(I) photoelectron spectra of the pyrochlore ruthenates are shown in Fig. 3. Close to the Fermi energy a weak peak can be discerned in each of the spectra; it is associated with ionization of Ru : $4d$ electrons. This merges with a stronger band peaking at about 4 eV binding energy deriving from the O : $2p$ electrons. The structure before the zero kinetic energy cutoff is due to secondary electrons.

In Fig. 4 we show expanded scans of the Ru : $4d$ regions of the spectra recorded at an instrumental resolution of 30 meV. Under these conditions the cutoff at zero binding energy in photoelectron spectra of metallic materials at room temperature is governed mainly by the Fermi–Dirac distribution function. In the present context the density of states at the Fermi energy may be gauged

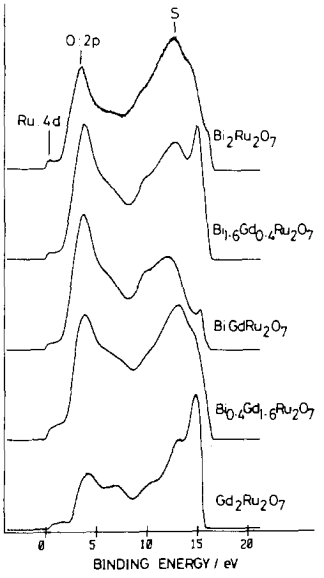

FIG. 3. Wide-scan He(I) photoelectron spectra of the pyrochlore ruthenates. Binding energies are given relative to the Fermi energy. Peaks due to Ru:4*d* states, O:2*p* states, and secondary electrons (*S*) are indicated in the figure.

by the tick marks lying 100 meV above and below the Fermi energy, this being roughly the energy interval in which the Fermi function increases from 5 to 95% of its maximum value. A striking feature of the spectra is the progressive increase in the density of states at the Fermi energy (as gauged by the height separation between the ticks) with increasing Bi content of the samples. There is no apparent discontinuous change in the spectra between $x = 1.4$ and $x = 1.6$, possibly indicating that the nonmetal-to-metal transition involves no discontinuous change in the density of states at the Fermi energy. This in turn favors a mechanism where the transition is mediated through disorder-induced electron localization in the nonmetallic regime.

Overall the data are consistent with the opening of a Mott–Hubbard gap as the Gd content of the samples increases. However, the spectra do not in themselves provide direct evidence for narrowing of the Ru : 4*d* conduction band with increasing Gd content; and, if anything, band broadening is apparent. This is due to the fact that final-state effects increasingly dominate the photoemission process as one moves toward the nonmetallic regime. As with $Y_2Ru_2O_7$ studied in our previous work (*3*), the Ru : 4*d* band for $Gd_2Ru_2O_7$ may be fitted to Gaussian profiles representing the final-state multiplet levels ($^4A_{2g}$, ^2E_g, $^2T_{1g}$, $^2T_{2g}$) accessible upon ionization of the $^3T_{1g}$ initial state. The multiplet components are differentiated in energy by final-state electron–electron repulsion effects and are individually broadened by coupling of the 4*d* photohole to longitudinal optical phonons of the pyrochlore lattice (*16*).

The evolution from metallic behavior in $Bi_2Ru_2O_7$ to nonmetallic behavior for $Gd_2Ru_2O_7$ is also strikingly apparent in the HREEL spectra of Fig. 5. As reported pre-

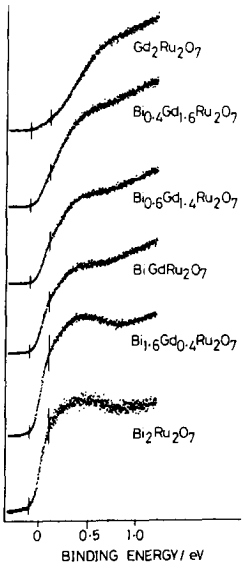

FIG. 4. Expanded scan of the Ru : 4*d* region in the He(I) photoelectron spectra of the pyrochlore ruthenates recorded at an instrumental resolution of 30 meV. Binding energies are given relative to the Fermi energy. The tick marks indicate an energy spread of 200 meV centered at the Fermi energy. The shape of these spectra at threshold conforms well to the Fermi–Dirac distribution function at room temperature.

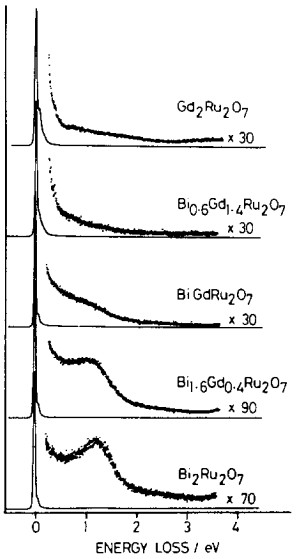

FIG. 5. HREEL spectra of the pyrochlore ruthenates excited with a 25-eV electron beam.

viously (*3*), the loss spectrum of $Bi_2Ru_2O_7$ contains a well-defined loss peak at 1.25 eV associated with excitation of the conduction-electron surface plasmon. This can be understood in terms of modified Drude theory with two-thirds occupancy of the t_{2g} band by electrons with an effective mass ratio 2.9. The plasmon loss moves to lower energy with increasing Gd content, indicating a parallel increase in the electron effective mass. Simultaneously the plasmon loss broadens, presumably as a result of an increase in the conduction-electron relaxation rate due to disorder-mediated scattering of the carriers. The upshot of this is that the plasmon loss becomes progressively less well defined as the Gd content increases and there is no discernible plasmon loss for $Gd_2Ru_2O_7$.

Although it is difficult to define the composition at which the plasmon structure collapses, the general behavior of the plasmon loss in HREELS provides important additional evidence that the transition to the nonmetallic state is dominated by electron correlation and the opening of a Mott–Hubbard gap. The red shift of the plasmon as one approaches the metal-to-nonmetal transition contrasts with the blue shift found in the temperature-dependent transition of Ti_2O_3 (*17*): in Ti_2O_3 an energy gap opens due to band decrossing within a one-electron band structure. The changes are, however, similar to those found for VO_2 where electron correlation is of crucial importance in driving the metal-to-nonmetal transition (*18*). The present study thus reinforces the view that the variation of plasmon frequency near a metal-to-nonmetal transition provides an important guide as to the mechanism of the transition.

To summarize then, the surface-sensitive techniques of UPS and HREELS both show clearly defined trends indicative of a progressive change between localized 4*d* electrons in $Gd_2Ru_2O_7$ and itinerant electrons in $Bi_2Ru_2O_7$. The Bi–Gd ruthenate pyrochlores thus provide an ideal model system with well-defined surface electronic structure in which to explore the influence of electron localization upon X-ray photoelectron spectra.

5. Ru: 3*d* Structure in X-Ray Photoelectron Spectra of Pyrochlore Ruthenates

Mg$K\alpha$ X-ray photoelectron spectra of the 3*d* core levels of the pyrochlore ruthenates recorded at an instrumental resolution of 1.2 eV are shown in Fig. 6. The spectrum of $Gd_2Ru_2O_7$ consists of a simple spin–orbit doublet with narrow, symmetric components: the $3d_{5/2}$ peak is at a binding energy of 282.2 eV relative to the Fermi energy. Bi substitution leads to broadening of the core signals through addition of a second spin–orbit doublet on the low-binding-energy side. The intensity of the second doublet increases with Bi content, and from $BiGdRu_2O_7$ through to $Bi_2Ru_2O_7$ the low-binding-energy doublet with peaks at 280.9

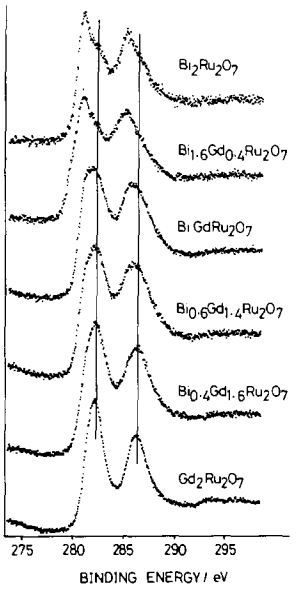

FIG. 6. X-Ray photoelectron spectra of pyrochlore ruthenates excited with unmonochromatized Mg$K\alpha$ radiation. Binding energies are given relative to the Fermi energy. Structure due to satellite radiation has been subtracted from the spectra. The solid lines show that the high-binding-energy components in the spectrum of $Bi_2Ru_2O_7$ correspond to the spin–orbit doublet of $Gd_2Ru_2O_7$.

eV ($3d_{5/2}$) and 285.2 eV ($3d_{3/2}$) dominates the spectra.

Interpretation of the complex core-level structure of the sort evident for $Bi_2Ru_2O_7$ has in the past proved to be controversial. However, as with other narrow-band metallic oxides, we believe that the structure arises from final-state screening effects as follows (*19, 20*). Ionization of a Ru core level produces an electrostatic perturbation at the ionized center. If the core-valence Coulomb interaction V_{cv} is greater than the width W of the one-electron conduction band, the perturbation will disengage one of the valence orbitals of the ionized atom from the conduction band. The resulting localized atomic state lies below the Fermi energy, and the site in question behaves as an electron trap akin to an impurity atom doped into the lattice. Two different final states then correspond to the alternative situations in which the trap state (i) is occupied by an itinerant conduction-band electron or (ii) remains empty. According to the model developed by Kotani and Toyazawa (*21*), the screened final state in which the trap becomes occupied should give rise to an asymmetric peak to the low-binding-energy side of the lifetime-broadened peak associated with the unscreened final state. More recently it has been suggested that screening in the high-binding-energy state arises from charge transfer from the O : 2p valence band so that the energy separation between the core-level peaks corresponds to the energy difference between the Fermi energy and the edge of the O : 2p valence band (*22*). In either case the spectra imply a progressive increase with Bi content and Ru : 4d bandwidth in the probability of screening by Ru : 4d electrons, a trend to be expected from simple model calculations.

The interpretation of the spectra in terms of final-state screening is in keeping with the solid-state properties of the ruthenates and with the changes evident in UPS and HREELS. In this respect it is superior to the alternative initial-state mixed-valence interpretation, which needs to invoke the cumbersome idea that following identical oxygen pretreatments $Bi_2Ru_2O_7$ remains contaminated with a reduced Ru oxide (which gives the low-binding-energy doublets) whereas isostructural $Gd_2Ru_2O_7$ does not.

6. Electronic Structure of RuO_2 in Relation to UPS and HREELS Data

The rutile structure of RuO_2 differs from that of the pyrochlores in that it is based on edge- (rather than corner-) sharing RuO_6 octahedra. However, in common with the pyrochlores the dominant O_h component of the ligand field splits the Ru : 4d orbitals into a more stable threefold-degenerate t_{2g} set and a less stable twofold-degenerate e_g

set. The metal *d* bands lie above a complex of bands of dominant O : 2*p* atomic character.

The simple qualitative considerations given above are confirmed by the band-structure calculations of Mattheis (*10*), which indicate an overall O : 2*p* bandwidth of order 6 eV with three distinct maxima in the density-of-states profile. Moreover the orthorhombic component of the crystal field associated with the D_{2h} (rather than O_h site symmetry) lifts the degeneracy of the t_{2g} orbitals and leaves one t_{2g} component relatively more stable than the other two. In the full band-structure calculation, however, dispersion of the *d* bands (arising mainly from Ru–O–Ru interactions) produces a density-of-states profile for the t_{2g} band with a distinct minimum at the Fermi energy corresponding to two-thirds occupancy of the band. In this sense the density-of-states profile does not correspond directly to the RuO_6 cluster energy levels (where one t_{2g} component is stabilized relative to the other two). The location of the Fermi energy at a minimum in the density of states for RuO_2 contrasts with the situation for d^1 and d^2 oxides such as VO_2 and MoO_2 where the Fermi energy sits in the bottom component of the t_{2g} band. For these materials distortion of the rutile structure through pairing along the *c* axis leads to a large shift of electronic states away from the Fermi energy, thereby providing a driving force for the distortion. Thus the stability of RuO_2 in the undistorted rutile structure is intimately connected with the detailed structure of the t_{2g} band and the location of the Fermi energy at a minimum in the density-of-states profile.

The photoelectron spectra shown in Fig. 7 provide elegant confirmation of the band-structure calculations. Both our UV photoemission spectra and X-ray excited valence-band spectra are in broad agreement with previously published data (*23–25*). As noted earlier (*25*), X-ray spectra are dominated by the partial 4*d* density of states and thus the Ru : 4*d* band is relatively stronger than at lower photon energy. The relationship between the O : 2*p* structure and the density-of-states calculations has been discussed in detail elsewhere (*24*) and will not be pursued further here. However, of crucial interest to the present study is the detailed shape of the Ru : 4*d* band evident in UV photoemission by virtue of our superior resolution. The expansion of the Ru : 4*d* band in the He(I) spectrum shown in Fig. 8 reveals that the Fermi energy cuts off the occupied density of states well away from the maximum in the *d* band profile.

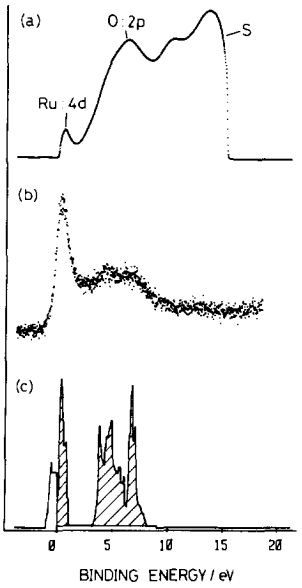

FIG. 7. Valence-band photoelectron spectra of RuO_2 excited with (a) He(I) discharge radiation ($h\nu$ = 21.2 eV) and (b) unmonochromatized Mg$K\alpha$ X rays ($h\nu$ = 1253.6 eV) shown alongside the density-of-states profile (c) taken from the band-structure calculations of Mattheis (*10*).

From spectra such as those shown in Fig. 8 it is possible to make estimates of the density of electronic states at the Fermi energy. Assuming that there is no change in photoionization matrix elements across the occupied part of the conduction band and that there is no modulation with photoelec-

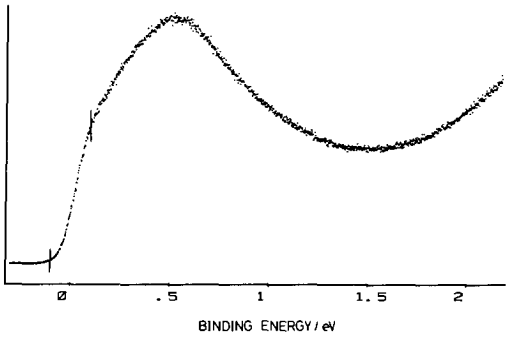

FIG. 8. Expanded scan of the Ru:4*d* band in the He(I) UV photoelectron spectrum of RuO_2 recorded at an instrumental resolution of 30 meV. The tick marks delineate an energy interval of 200 meV centered at the Fermi energy.

tron energy in the density of final states, it is possible to normalize the area of the Ru:4*d* band to the electron concentration implied by the d^4 ruthenium configuration. The measured height of the Fermi edge discontinuity in UPS then corresponds to a density of electronic states at the Fermi energy of 2.1 states/eV-Ru atom. This value is in excellent agreement with values of 1.9 states/eV-Ru atom from the band-structure calculations (*10*) and of 2.4 states/eV-Ru atom from an interpretation of the measured electronic contribution to the specific heat that ignores possible enhancement by electron–electron or electron–phonon interactions (*26*). Thus UPS probes a conduction band whose density-of-states profile accords well with theory and an experimental technique sensitive to bulk conduction-electron concentration. In contrast to materials such as $LiTi_2O_4$ (*27*) and ruthenates just to the metallic side of a metal–nonmetal transition (*3*), the low height of the Fermi-edge discontinuity in UPS appears to reflect features of the one-electron band structure rather than final-state electron–electron or electron–phonon effects. Moreover there is no indication of perturbation of the conduction electrons close to the surface due to oxidation or reduction of the sample.

These conclusions are further reinforced by the electron-energy-loss spectra of Fig. 9. It is seen in this figure that a prominent loss feature appears in the spectra at an energy of 1.78 eV independent of the beam energy in the range 10–500 eV. From a comparison with the loss spectra of the ruthenates and related materials such as ReO_3 (*28*), it appears that this feature is due to excitation of the surface plasmon of RuO_2. The position of the surface-plasmon loss accords well with the optical reflectivity data of Goel *et al.* (*29*). These authors found that $Re[\varepsilon(\omega)] = 0$ at 1.8 eV, an energy to be equated with the screened bulk-plasmon frequency (that is, the plasma frequency of the carriers in a background medium whose dielectric constant is determined by the interband excitations at higher energy). It appears from their paper

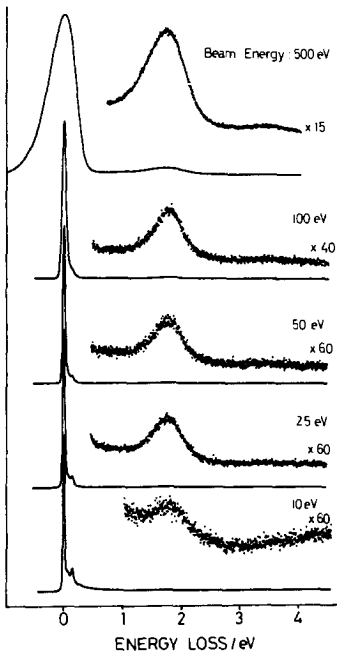

FIG. 9. Electron-energy-loss spectra of RuO_2 excited at differing electron beam energies between 10 and 500 eV. The 500-eV spectrum was excited with the unmonochromated electron source of the ESCALAB LEED gun. Other spectra were excited with a monochromated electron source.

that the corresponding surface-plasmon frequency where $Re[\varepsilon(\omega)] = -1$ lies very close to the loss frequency in our EELS experiments.

The point crucial to our present discussion is that the effective penetration depth λ of the surface-plasmon excitation in EELS is governed by the electron-beam velocity v normal to the surface relative to the frequency ω of the surface excitation (*30*):

$$\lambda = v/\omega.$$

Within the energy range of our EELS experiments λ thus increases from 7 Å at 10 eV to 50 Å at 500 eV. Now the plasma frequency is sensitively dependent upon the conduction-electron concentration, and the invariance upon changing the electron-beam energy therefore implies that over the depth range discussed above the carrier concentration is equal to its bulk value.

To summarize, both UPS and EELS probe a conduction-electron concentration in RuO_2 equal to its bulk value: there is no evidence for removal or addition of electrons to the conduction band by oxidation or reduction of the sample surface.

7. Ru: 3*d* X-Ray Photoelectron Spectra of RuO_2

Ru: 3*d* structure in the Mg*Kα* X-ray photoelectron spectrum of RuO_2 is shown in Fig. 10. This spectrum is similar to spectra reported by Kim and Winograd (*7*) and by Kotz and co-workers (*8, 9*); it consists of two overlapping spin–orbit doublets, the $3d_{5/2}$ components appearing at 280.8 and 282.6 eV. The low-binding-energy components dominate the spectrum. In previous work the observation of two distinct Ru: 3*d* binding energies was taken to indicate partial oxidation of the RuO_2 surface; the 280.8-eV component was associated with the Ru(IV) ions of RuO_2 and the higher-binding-energy 282.6-eV component with

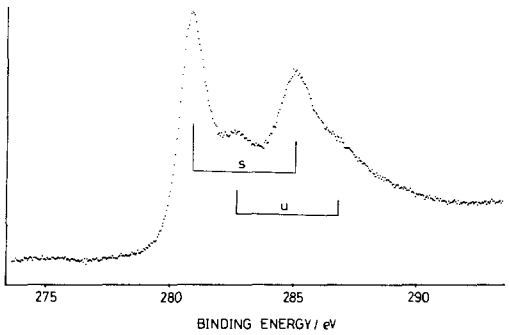

FIG. 10. Mg*Kα* X-ray photoelectron spectrum of RuO_2 following removal of structure due to satellite radiation. The bars indicate the positions of overlapping spin–orbit doublets due to screened and unscreened final states.

Ru(VI) ions in an "RuO_3" oxidized surface layer (*7–9*).

We do not believe the initial-state mixed-valence interpretation. The striking similarity of the spectrum with that of $Bi_2Ru_2O_7$ suggests instead that, as with metallic pryochlore ruthenates, final-state screening by Ru: 3*d* electrons is responsible for the appearance of the low-binding-energy peaks; the high probability of final-state screening is consistent with the good metallic conductivity of RuO_2. The problems with the mixed-valence interpretation given elsewhere are threefold. First, the oxide "RuO_3" postulated to account for the high-binding-energy peaks does not exist as a discrete solid phase and its existence as an ill-defined surface species is highly questionable. Second, our own studies of nonmetallic Ru(IV) oxides establish a typical Ru: 3*d* binding energy of 282.2 eV. Thus the high-binding-energy peak of RuO_2 at 282.6 eV corresponds to Ru(IV) unscreened by metallic conduction electrons, and the only coherent mixed-valence interpretation involves the dominant low-energy peaks arising from a lower ruthenium oxide such as Ru_2O_3 or RuO. Again these are not well-defined Ru oxide phases and should not be invoked unless there are compelling

reasons; their formation on a surface prepared by annealing in oxygen is scarcely credible. Third, the UPS and EELS data of our own study are completely inconsistent with oxidation or reduction of the RuO_2 surface.

In summary, the Ru : 3*d* XPS of RuO_2 appears typical of a narrow-band metallic oxide. The only ambiguity to emerge from our own study is that even after sample cleaning we observe a double peak structure in the O : 1*s* region in XPS with a strong satellite some 1.6 eV below the main peak. This may conceivably arise from plasmon excitation, although it is much stronger than expected from this mechanism. We note, however, that complex structures in O : 1*s* XPS of single-crystal RuO_2 exhibiting sharp (1 × 1) LEED patterns (presumably a signature of a well-ordered, stoichiometric surface) exhibit similar structure (*31*). Thus an interpretation in terms of final-state effects deserves further consideration.

Acknowledgments

The equipment used was funded by the SERC. We are grateful to Shell Research for the award of a CASE studentship to P.J.T.

References

1. W. B. Ryden, A. W. Lawson, and C. Sartan, *Phys. Rev. B* **1,** 1444 (1974).
2. M. A. Subramanian, G. Aravamdan, and G. V. Subba Rao, *Progr. Solid State Chem.* **15,** 55 (1983).
3. P. A. Cox, R. G. Egdell, J. B. Goodenough, A. Hamnett, and C. C. Naish, *J. Phys. C* **16,** 6221 (1983).
4. R. G. Egdell, J. B. Goodenough, A. Hamnett, and C. C. Naish, *J. Chem. Soc. Faraday Trans. 1* **79,** 893 (1983).
5. S. Trassati and G. Lodi, *in* "Electrodes of Conductive Metal Oxides" (S. Trassati, Ed.), Part B, p. 521, Elsevier, New York (1981).
6. H. S. Horowitz, J. M. Longo, and J. I. Haberman, U.S. Patent 4146458 (1979).
7. K. S. Kim and N. Winograd, *J. Catal.* **35,** 66 (1974).
8. H. J. Lewerenz, S. Stucki, and R. Kotz, *Surf. Sci.* **126,** 893 (1983).
9. R. Kotz, H. J. Lewerenz, and S. Stucki, *J. Electrochem. Soc.* **130,** 825 (1983).
10. L. F. Mattheis, *Phys. Rev. B* **13,** 2433 (1976).
11. D. B. Rogers, R. D. Shannon, A. W. Sleight, and J. C. Gillson, *Inorg. Chem.* **8,** 841 (1969).
12. A. F. Orchard and G. Thornton, *J. Electron Spectrosc.* **13,** 27 (1978).
13. J. B. Goodenough, A. Hamnett, and D. Telles, *in* "The Mott Birthday Present" (H. Fritzsche and D. Adler, Eds.), Plenum, New York (1985).
14. D. Telles, M.Sc. thesis, Oxford (1984).
15. P. A. Cox, *Struct. Bond.* **24,** 59 (1975).
16. C. Kunz, *in* "Photoemission in Solids" (L. Ley and M. Cardona, Eds.), Springer-Verlag, Berlin (1979).
17. G. Campagnoli, A. Giustinetti, A. Stella, and E. Tosatti, *Phys. Rev. B* **20,** 2217 (1979).
18. A. Bianconi, S. Stizza, and R. Bernadini, *Phys. Rev. B* **24,** 4406 (1981).
19. N. Beatham, P. A. Cox, R. G. Egdell, and A. F. Orchard, *Chem. Phys. Lett.* **69,** 479 (1980).
20. J. N. Chalzalviel, M. Campagna, G. K. Wertheim, and H. R. Shanks, *Phys. Rev. B* **16,** 697 (1977).
21. A. Kotani and Y. Toyazawa, *J. Phys. Soc. Japan* **37,** 912 (1974).
22. G. K. Wertheim, *Phys. Rev. B,* in press.
23. N. Beatham and A. F. Orchard, *J. Electron Spectrosc.* **16,** 77 (1979).
24. R. R. Daniels, G. Magaritondo, C. A. Georg, and F. Levy, *Phys. Rev. B* **29,** 1813 (1984).
25. J. Riga, C. Tenret-Noel, R. Caudano, and J. J. Pireaux, *Phys. Sci.* **16,** 351 (1977).
26. B. C. Passenheim and D. C. McCollum, *J. Chem. Phys.* **51,** 320 (1969).
27. P. P. Edwards, R. G. Egdell, I. Fragala, J. B. Goodenough, M. R. Harrison, E. G. Scott, and A. F. Orchard, *J. Solid State Chem.* **54,** 127 (1984).
28. R. E. Dietz, M. Campagna, J. N. Chalzalviel, and H. R. Shanks, *Phys. Rev. B* **17,** 3790 (1978).
29. A. K. Goel, G. Shorinko, and F. H. Pollak, *Phys. Rev. B* **24,** 7342 (1981).
30. H. Ibach and D. L. Mills, "Electron Energy Loss Spectroscopy and Surface Vibrations," Academic Press, New York (1982).
31. W. E. O'Grady, Lj. Atanasoska, F. H. Pollak, and H. L. Park, *J. Electroanal. Chem.* **178,** 61 (1984).